Journal of Alloys and Compounds 898 (2022) 162874

Contents lists available at ScienceDirect

Journal of Alloys and Compounds

journal homepage: www.elsevier.com/locate/jalcom

High-pressure synthesis of boron-rich chalcogenides $B_{12}S$ and $B_{12}Se$

Kirill A. Cherednichenko[a,b], Vladimir A. Mukhanov[a], Aleksandr Kalinko[c,d], Vladimir L. Solozhenko[a,*,1]

[a] LSPM–CNRS, Université Sorbonne Paris Nord, Villetaneuse 93430, France
[b] Department of Physical and Colloid Chemistry, Gubkin University, Moscow 119991, Russia
[c] Photon Science – Deutsches Elektronen-Synchrotron (DESY), 22607 Hamburg, Germany
[d] Institute of Solid State Physics, University of Latvia, Riga LV-1063, Latvia

ARTICLE INFO

Article history:
Received 29 July 2021
Received in revised form 10 November 2021
Accepted 18 November 2021
Available online 24 November 2021

Keywords:
Boron-rich chalcogenides
High-pressure synthesis
Crystal structure
Raman spectra

ABSTRACT

Two boron-rich chalcogenides $B_{12}S$ and $B_{12}Se$ isostructural to α-rhombohedral boron were synthesized by chemical reaction of the elements at high-pressure – high-temperature conditions. The crystal structures and stoichiometries of both compounds were confirmed by Rietveld refinement of synchrotron X-ray diffraction data and elemental analysis. The experimental Raman spectra of $B_{12}S$ and $B_{12}Se$ were investigated for the first time. All observed Raman bands have been attributed to the theoretically calculated phonon modes, and the mode assignment has been performed.

1. Introduction

Boron-rich compounds isostructural to the α-rhombohedral boron (α-B_{12}) have become the subject of extensive theoretical [1–11] and experimental [12–23] studies due to their unusual properties and potential technical applications [14,18,24]. One of the most attractive features of boron-rich compounds is their outstanding mechanical properties. For instance, the reported Vickers hardness values of boron suboxide ($B_{12}O_2$) vary from 24 to 45 GPa [25–31]. Thus, boron suboxide is believed to be the hardest known oxide. Numerous works have been devoted to the investigation of its phase stability [3,32], compressibility [32–34], phonon [35–37] and thermal [34,38] properties, etc. However, other boron-rich chalcogenides, unlike boron suboxide, are still poorly studied.

Up to now, there have been only a few reports on the synthesis of boron subsulfide ($B_{12}S_x$) [39–41] and boron subselenide ($B_{12}Se_x$) [42]. In all these studies boron chalcogenides were synthesized by the chemical reaction between elemental boron and sulfur/selenium in graphite or tantalum crucibles at high temperatures (1200–1600 °C) in the Ar atmosphere. The chalcogen content "x" varies from 0.9 to 1.3 in $B_{12}S_x$, and from 0.9 to 1.1 in $B_{12}Se_x$. This is not surprising taking into account relatively low boiling temperatures of elemental sulfur (718 K) and selenium (958 K). Thus, the synthesis conditions (e.g. starting reagents ratios, maximum temperature, heating time, etc.) influence significantly the final stoichiometry of the products.

The loss of elemental sulfur and selenium during the high-temperature synthesis of boron chalcogenides can be prevented by applying high pressure. For instance, the high-pressure – high-temperature (HP-HT) synthesis provided a reproducible stoichiometry of many boron-rich compounds, such as $B_{12}O_2$ [21], $B_{13}N_2$ [17], $B_{50}N_2$ [43] and $B_{12}As_2$ [44], as well as recently synthesized new orthorhombic B_6S and B_6Se [45]. Thus, there are strong grounds to believe that HP-HT synthesis can ensure the reproducible chemical composition of boron-rich chalcogenides as well.

In the present work, we performed HP-HT synthesis of $B_{12}S$ and $B_{12}Se$. The crystal structures and chemical compositions of both boron-rich chalcogenides were confirmed by Rietveld refinement of the powder X-ray diffraction data and elemental analysis. The Raman spectra of both compounds have been experimentally observed for the first time. Based on *ab initio* calculations, we assigned all observed Raman bands.

2. Experimental

Polycrystalline samples of $B_{12}S$ and $B_{12}Se$ were synthesized at 6 GPa and 2500 K by reaction of elemental boron (Grade I ABCR)

* Corresponding author.
E-mail address: vladimir.solozhenko@univ-paris13.fr (V.L. Solozhenko).
[1] orcid.org/0000–0002-0881–9761

https://doi.org/10.1016/j.jallcom.2021.162874
0925-8388/

with sulfur/selenium (both Alfa Aesar, 99.5%) powders mixed in 15:1/18:1 molar ratios. The compacted mixtures of starting reagents were loaded in hBN capsules (to isolate the reaction mixture from graphite heater) and placed in the high-temperature assembly of a toroid-type high-pressure apparatus. After reaching the required pressure, the reaction mixtures were heated at 2500 K for 3 min, then gradually cooled down to 1500 K for 10 min and quenched. In order to remove unreacted boron, the recovered samples were grinded in mortar and treated with 3 N nitric acid (ACS, Alfa Aesar) for 20 min at 370 K, washed by deionized water and dried at 400 K.

The structure of as-synthesized compounds was studied by angle-dispersive powder X-ray diffraction at Swiss-Norwegian Beamline BM01, ESRF [46]. The wavelength of the monochromatic beam from a bending magnet was set to 0.6866 Å. Diffraction patterns of fine powder samples were acquired during the 20 s in Debye-Scherrer geometry with rotating quartz-glass capillary using PILATUS 2M detector (high purity LaB_6 was used as an internal standard). The crystal structures of both compounds were refined using Maud software [47] (Fig. 1).

The chemical composition of $B_{12}S$ and $B_{12}Se$ powders was studied by energy-dispersive X-ray analysis using scanning electron microscopes FEI Quanta 200 F and TESCAN MIRA3 both equipped with SDD X-Max^n 80 EDS system (Oxford Instruments).

Raman spectra were measured in the 100–1600 cm^{-1} range at ambient conditions using Horiba Jobin Yvon HR800 spectrometer calibrated with single-crystal cubic Si at room temperature. In order to check for possible resonant effects and/or photoluminescence, the measurements were performed at two different excitation wavelengths: 473 nm and 633 nm. None of those phenomena have been observed for both compounds.

3. Computational

The lattice parameters and atomic fractional coordinates of trigonal *R*-3*m* $B_{12}S$ and $B_{12}Se$ phases were optimized using a linear combination of atomic orbitals (LCAO) method implemented in CRYSTAL17 code [48]. The starting unit cell parameters and atom coordinates were taken from the experimental data. Improved all-electron double-zeta valence basis sets augmented by one set of polarization functions (pob-DZVP-rev2) [49] were chosen for boron, sulfur and selenium atoms. The accuracy of the calculation of the bielectronic Coulomb and exchange series was controlled by the set of tolerances, which were set to 10^{-8}, 10^{-8}, 10^{-8}, 10^{-8}, and 10^{-16}. The Monkhorst-Pack scheme [50] for an 8×8×8 k-point mesh was used to integrate the Brillouin zone. Self-consistent field calculations were performed for hybrid DFT/HF WCGGA-PBE-16% functional [51,52]. The percentage of 16% defines the Hartree-Fock admixture in the exchange part of DFT functional. The tolerance for the total energy change was set to 10^{-10}.

To calculate $B_{12}S$ and $B_{12}Se$ phonon frequencies the direct (frozen-phonon) method implemented in CRYSTAL17 code [53,54] was used. Raman intensities were calculated by using a coupled-perturbed Hartree–Fock/Kohn–Sham approach [54,55] The parameters of the optimized unit cell as well as atomic coordinates are collected in Table 4. Raman spectra were constructed by using the transverse optical (TO) modes and by adopting a pseudo-Voigt functional form [53] with a full width half maximum parameter set to 1.

4. Results and discussions

4.1. Crystal structures of $B_{12}S$ and $B_{12}Se$

As typical α-B_{12}-related compounds, boron subsulfide and boron subselenide have rhombohedral symmetry (*R*-3*m* space group). The 5-order polynomial was employed to approximate the background. According to 2D X-ray diffraction images (see Fig. 1) the samples of both compounds were finely and uniformly powdered, and therefore the application of texture and/or strain models in Rietveld refinement was not needed. The refined lattice parameters of $B_{12}S$ and $B_{12}Se$ were found to be in good agreement with the literature data (Table 1). The unit cells of both compounds contain two independent boron atoms (in *18h* Wyckoff positions) and one sulfur/selenium atom (in *6c* Wyckoff position). All atomic coordinates and bond lengths are presented in Table 2. The slightly distorted B_{12}-icosahedra are placed in the corners of the unit cell and on one of the unit cell main diagonals. The inter-icosahedral B-B bonds are longer than inter-icosahedral ones, that is typical for the majority of boron-rich compounds related to α-boron (e.g. B_6O [56], $B_{12}S_x$ [39–41], $B_{12}Se_x$ [42]). S/Se atoms have a tetrahedral environment, including three B atoms belonging to three different boron icosahedra and one S/Se atom. According to the Rietveld refinement, the occupancies of *6c* sites by S and Se atoms were found to be 55% and 52%, respectively. Since all boron atoms constitute B_{12}-icosahedra, the occupancies of *18h* sites were fixed to 1.0 by default. The results of Rietveld refinement are in good agreement with energy-dispersive X-ray spectroscopy data (Fig. 2): the elemental compositions of $B_{12}S_x$ and $B_{12}Se_x$ are 92.5(1) at% B and 7.5(1) at% S and 92.6(1) at% B and 7.4(1) at% Se, i.e. x≈1 for both compounds. The final reliability factors (R_{wp}) were converged to 2.4 for $B_{12}S$ and 0.5 for $B_{12}Se$, which indicates the excellent refinement level (Fig. 1).

The occupancies of *6c* sites by S/Se atoms in $B_{12}S$ and $B_{12}Se$ refined in our study are close to the values obtained previously [40–42] (Table 1). An attempt to place a single S/Se atom in *3b* site (between two *6c* sites) as it was proposed by Matkovich [39] resulted in not satisfactory profile fit convergence of the Rietveld refinement. Moreover, a replacement of the S/Se atom by B atom in *6c* positions as it was done previously (e.g. $B_{12}Se_{2-x}B_x$) [42] led to significant refinement deteriorations and, hence, high R_{wp} values. Thus, despite the partial occupancies of *6c* sites in $B_{12}S/B_{12}Se$ unit cells, the results of our Rietveld refinement exclude a possibility of the S/Se atoms "sliding" to *3b* Wyckoff position or their partial replacement by boron atoms.

The ~50% occupancy of *6c* site in $B_{12}S$ and $B_{12}Se$ induces some structural disorder since there is one S/Se atom per rhombohedral unit cell occupying only one of two the *6c* sites (or 3 S/Se atoms per hexagonal unit cell occupying three of six *6c* sites) (Fig. 3). A partial occupancy of *6c* sites was first discovered by Bolmgren et al. [42]. The proposed explanation was: Se-Se interatomic distance (1.931 Å) is too short compared to double Se covalent radius (2 ×1.20 Å). In other words, $B_{12}Se$ unit cell is too small to accommodate two Se atoms. Taking into account the Se-Se distance of 2.02 Å found in present study (that is shorter than double covalent radius of Se) the same logic was employed. However, it cannot be applied in the case of $B_{12}S$: S-S interatomic distance is 2.23 Å, whereas the sulfur covalent radius is 1.05 Å. The nature of the partial occupancies of *6c* sites in $B_{12}S$ remains unclear. As follows from Table 1 and Fig. 3, the larger values of *6c* site occupancy in boron subsulfides expectedly lead to the expansion of the lattice parameters (particularly, along the *c*-axis) and increase of the calculated densities. Unlike boron subsulfides, larger values of *6c* site occupancy in boron subselenide surprisingly result in the lower calculated density and shrinking of the unit cell along the *c*-axis (Table 1).

4.2. Raman spectroscopy study of $B_{12}S$ and $B_{12}Se$

Unlike recently synthesized orthorhombic boron-rich chalcogenides, *o*-B_6S and *o*-B_6Se, [57] the Raman spectra of rhombohedral $B_{12}S$ and $B_{12}Se$ contain broad bands in the 150–1250 cm^{-1} range (Fig. 4). The both Raman spectra are noisy which can be explained by

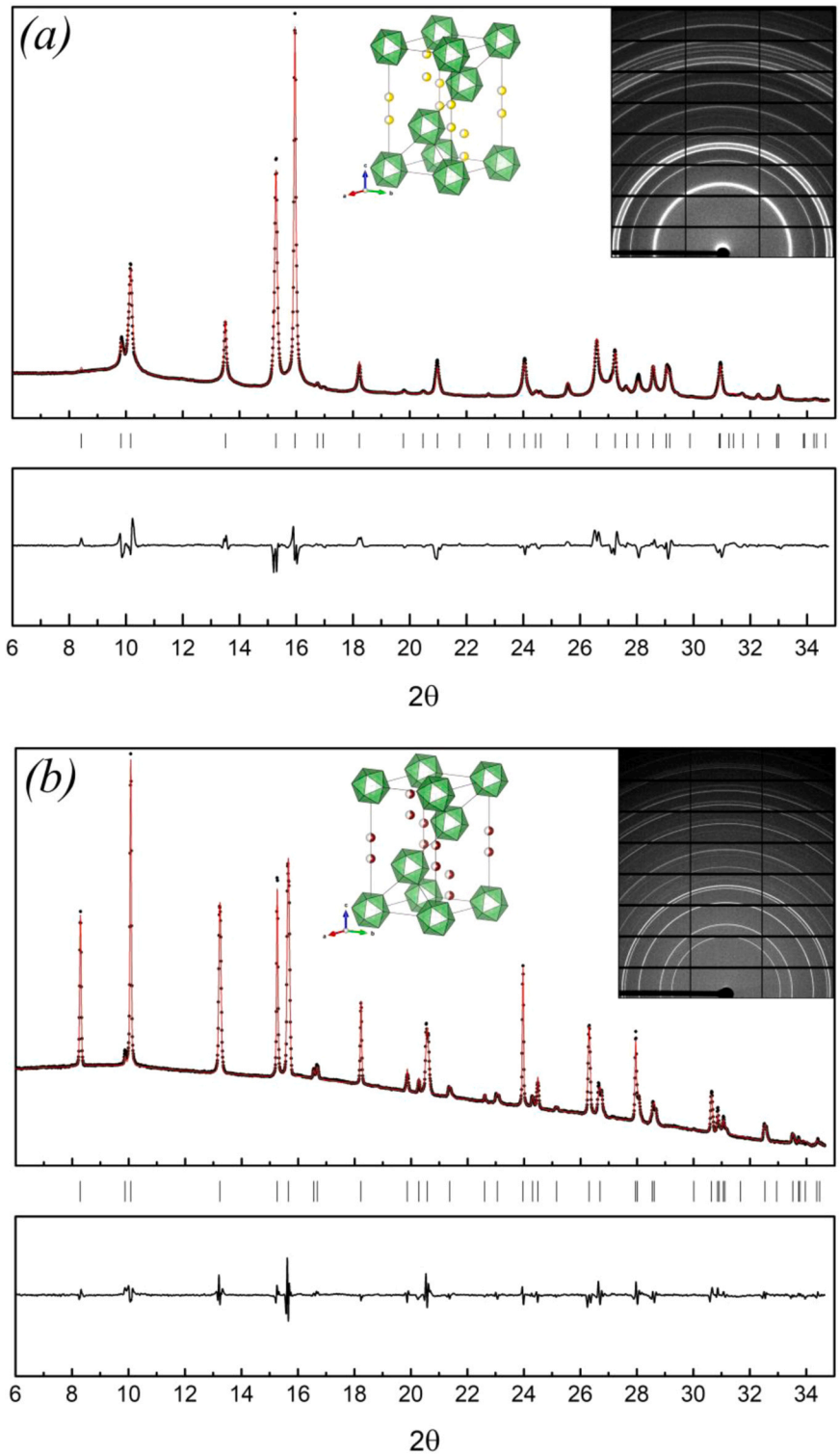

Fig. 1. Rietveld full profile refinement fits of powder X-ray diffraction ($\lambda = 0.6866$ Å) patterns of $B_{12}S$, $R_{wp} = 2.4$ (*a*) and $B_{12}Se$, $R_{wp} = 0.5$ (*b*). The insets present the 2D X-ray diffraction images and unit cells of both compounds in hexagonal setting.

Table 1
Lattice parameters, *X-X* interatomic distances (*X*=S, Se), occupation of *6c* sites by *X* atoms and X-ray densities of $B_{12}S$ and $B_{12}Se$: present work (*pw*) and literature data.

Compound	*a*, Å	*c*, Å	X-X, Å	Occup., %	ρ, g/cm^3	Reference
$B_{12}S$	**5.8196(2)**	**11.9653(5)**	**2.23(2)**	**55**	**2.34**	*pw*
	5.80	11.90	2.450	50[a]	2.33	[39]
	5.810(2)	11.94(2)	–	48.5	–	[40]
	5.8624(9)	12.147(4)	–	65	–	
	5.8379(6)	12.036(1)	–	59.9	2.36	[41]
	5.8307(5)	12.028(2)	–	60.9	2.37	
	5.8273(3)	12.025(2)	2.381	62	2.39	
$B_{12}Se$	**5.9385(1)**	**11.9144(2)**	**2.02(3)**	**52**	**2.90**	*pw*
	5.9041(4)	11.947(1)	1.931	46.9[b]	2.97	[42]

[a] S atom occupies *3b* position (occupation is 100%), thus stoichiometry of compound is $B_{12}S$. Here, for the sake of comparison, one S atom was sheared between two *6c* sites, thus, giving occupation of 50%.
[b] the stoichiometry of the compound is $B_{12}Se_{2-x}B_x$.

Table 2
The atomic coordinates, B_{iso} factors, sites occupancies, structures and bond lengths of $B_{12}S$ and $B_{12}Se$.

	Atom label (Wyckoff)	*x*	*y*	*z*	B_{iso}, Å^2	Site occupancy
$B_{12}S$	S1 (*6c*)	0.0000	0.0000	0.0934(2)	3.1(1)	0.55
	B1 (*18 h*)	0.4419(2)	0.5581(2)	0.0437(2)	3.6(1)	1.0 [f]
	B2 (*18 h*)	0.5004(3)	0.4996(3)	0.1948(2)	3.9(1)	1.0 [f]
	S-S, Å		2.230(20)			
	B2-S, Å		1.790(10)			
	B1-B2, Å		1.862(14)			
	B1-B1^{intra}, Å		1.890(30)			
	B1-B1^{inter}, Å		1.590(30)			
	B2-B2, Å		1.776(9)			
	Atom label (Wyckoff)	*x*	*y*	*z*	B_{iso}, Å^2	Site occupancy
$B_{12}Se$	Se1 (*6c*)	0.0000	0.0000	0.08501(1)	1.5(1)	0.52
	B1 (*18 h*)	0.4360(2)	0.5640(2)	0.0481(3)	2.0(1)	1.0 [f]
	B2 (*18 h*)	0.4955(3)	0.5045(3)	0.1953(3)	1.5(0)	1.0 [f]
	Se-Se, Å		2.020(30)			
	B2-Se, Å		1.872(12)			
	B1-B2, Å		1.812(14)			
	B1-B1^{intra}, Å		1.830(30)			
	B1-B1^{inter}, Å		1.750(30)			
	B2-B2, Å		1.802(10)			

[f] the atom site occupancies were fixed to 1.0
^{inter} inter-icosahedral B1-B1 bonds
^{intra} intra-icosahedral B1-B1 bonds

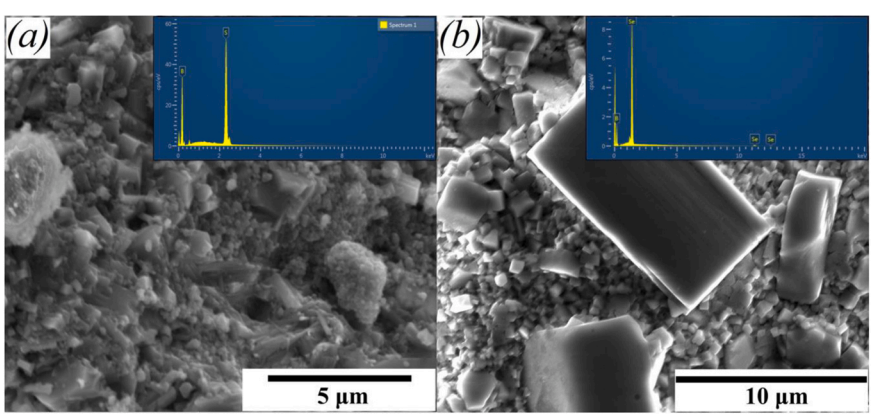

Fig. 2. SEM micrographs of $B_{12}S$ (*a*) and $B_{12}Se$ (*b*); the insets present the corresponding EDS spectra.

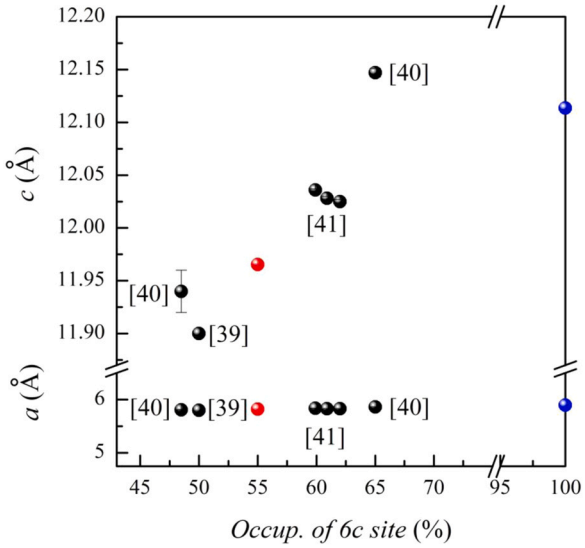

Fig. 3. Comparison of $B_{12}S$ lattice parameters versus occupation of *6c* site by S atom obtained in present work (XRD and theoretical data are presented by red and blue spheres, respectively) with literature data (black spheres).

disordered structure of both compounds. According to the symmetry analysis, the acoustic and optic modes of boron-rich chalcogenides at Γ point can be presented as follows:

$$\Gamma_{acoustic} = A_{2u} + E_u$$

$$\Gamma_{optic} = 5A_{1g} + 4A_{2u} + 6E_u + 7E_g + 2A_{1u} + 2A_{2g}$$

Table 3
The frequencies of the experimentally observed Raman bands at 633 nm excitation wavelength (ω_0) and Raman active modes predicted by CRYSTAL17 (ω_t), respectively. The overlapped bands groups (or too large bands) observed in experimental Raman spectra are presented by the corresponding frequency regions.

$B_{12}S$			$B_{12}Se$		
ω_0, cm^{-1}	ω_t, cm^{-1}	modes	ω_0, cm^{-1}	ω_t, cm^{-1}	modes
319.2	323.3	A_{1g}	–	199.6	A_{1g}
355.3	355.2	E_g		231.5	E_g
458.2	486.2	E_g	449.6	477.9	E_g
625.0	677.2	A_{1g}	645.3	644.6	A_{1g}
640–770	731.8	E_g	660–730	697.5	E_g
	754.1	E_g		711.7	E_g
	761.9	A_{1g}	741.1	745.7	A_{1g}
813.2	824.8	E_g	812.1	804.3	E_g
944–1170	1039.2	A_{1g}	900–1135	1020.7	E_g
	1047.6	E_g		1024.1	A_{1g}
	1093.7	A_{1g}		1038.4	A_{1g}
	1095.1	E_g		1062.8	E_g

where $5A_{2u} + 7E_u$ are IR active modes; $5A_{1g} + 7E_g$ are Raman active modes; $2A_{2g}$ and $2A_{1u}$ modes are both Raman and IR inactive for the D_{3d} point group.

The theoretically predicted Raman spectra of $B_{12}S$ and $B_{12}Se$ (at T = 0 K) are presented in Fig. 4 (the positions of the theoretical Raman bands peaks are denoted by red dashed lines). The wavenumbers of the calculated Raman active phonon modes (ω^t) and the experimentally observed Raman bands (ω_0) are collected in Table 3. As it follows from Fig. 4 and Table 3, the theoretical and experimental data are in good agreement (as it was also observed in our

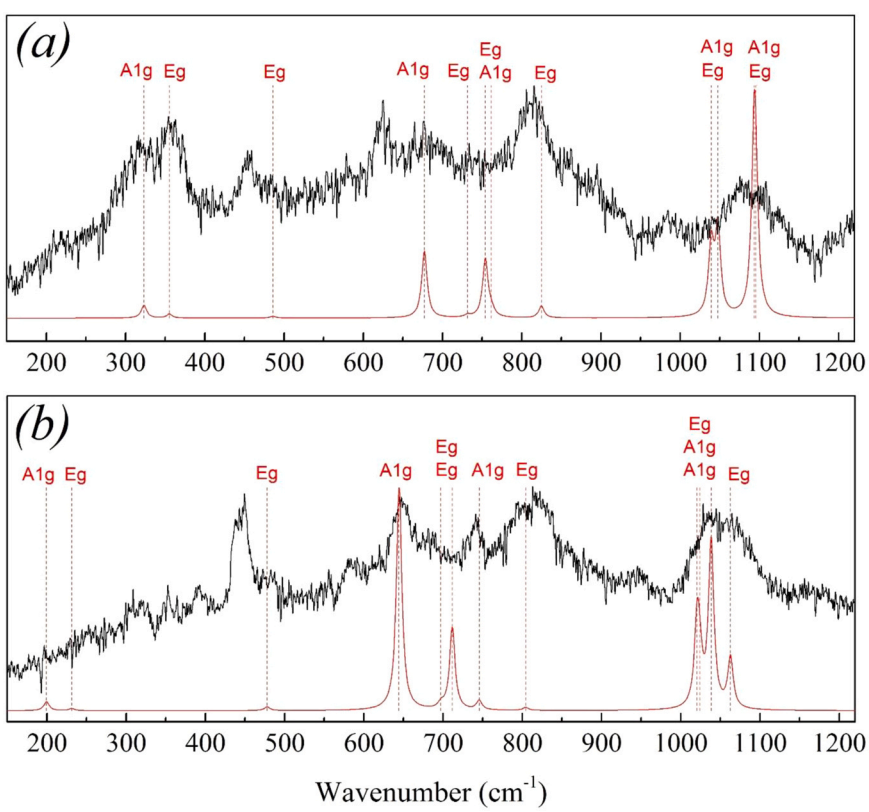

Fig. 4. Experimentally observed (black) and LCAO-calculated (red) Raman bands of $B_{12}S$ (*a*) and $B_{12}Se$ (*b*) at ambient conditions. The positions of the predicted Raman peaks are traced by red dashed lines, the corresponding phonon modes are indicated. (For interpretation of the references to colour in this figure legend, the reader is referred to the web version of this article.)

Table 4
The lattice parameters of the optimized unit cell, atomic coordinates and sites occupancies of $B_{12}S$ and $B_{12}Se$.

	Atom label (Wyckoff)	*x*	*y*	*z*	Site occupancy
$B_{12}S$	S1 (*6c*)	0.0000	0.0000	0.1186	1.0 [f]
	B1 (*18 h*)	0.4366	-0.4366	0.0479	1.0 [f]
	B2 (*18 h*)	-0.1787	0.1787	0.1400	1.0 [f]
	a, Å	5.8966			
	c, Å	12.1135			
	V, Å^3	364.76			
	Atom label (Wyckoff)	*x*	*y*	*z*	Site occupancy
$B_{12}Se$	Se1 (*6c*)	0.0000	0.0000	0.1217	1.0 [f]
	B1 (*18 h*)	0.4352	-0.4352	0.0467	1.0 [f]
	B2 (*18 h*)	-0.1836	0.1836	0.1397	1.0 [f]
	a, Å	6.0496			
	c, Å	12.1603			
	V, Å^3	385.42			

[f] all calculations were performed for site occupancies fixed to 1.0

previous Raman studies [58,59]): the average difference between experimental and theoretical data is less than 3.5% for $B_{12}S$ (with a maximum value of 6.1% for 486.2 cm^{-1} mode) and 1.5% for $B_{12}Se$ (with a maximum value of 6.3% for 477.9 cm^{-1} mode).

Using the visualization procedure built-in MOLDRAW software [60], the theoretically predicted phonon modes were attributed to the oscillations of two main structural elements of $B_{12}X$, where X = S/Se: triangle composed of 'B1' polar boron atoms (further, $(B1)_3$ unit) and X atom linked with three different 'B2'equatorial boron atoms (further, X-$(B2)_3$ unit) of B_{12}-icosahedra (Fig. 5).

The low-frequency A_{1g} and E_g modes (323.3 cm^{-1} and 355.2 cm^{-1} for $B_{12}S$ and 199.6 cm^{-1} and 231.5 cm^{-1} for $B_{12}Se$) were referred to S/Se atoms oscillations (parallel and perpendicular to the *c*-axis) and the corresponding slight distortions in B_{12}-icosahedra. As it follows from Fig. 3*b*, A_{1g} and E_g modes have not been experimentally observed for $B_{12}Se$ in the 150–400 cm^{-1} range. The most probable explanation for this phenomenon may be the low intensity of the corresponding Raman bands and the low signal-to-noise ratio of the whole Raman spectrum.

The E_g modes of $B_{12}S$ (458.2 cm^{-1}; 731.8 cm^{-1}) and $B_{12}Se$ (449.6 cm^{-1}; 697.5 cm^{-1}) can be assigned to the tilting of $(B1)_3$ units and twisting oscillations of boron atoms in X-$(B2)_3$ unit leading to the tilting of the whole icosahedra around different unit cell directions. Meanwhile, the E_g modes of $B_{12}S$ (754.1 cm^{-1}; 824.8 cm^{-1}; 1047.6 cm^{-1}; 1095.1 cm^{-1}) and $B_{12}Se$ (711.7 cm^{-1}; 804.3 cm^{-1}; 1020.7 cm^{-1}; 1062.8 cm^{-1}) correspond to symmetric and asymmetric stretching/twisting oscillations of B–B bonds and stretching/rocking oscillations of B–X bonds in $(B1)_3$ and X-$(B2)_3$ units, respectively. It might be roughly assumed that vibrations of $(B1)_3$ units lead basically to the distortions of the icosahedra and, thus, to distortions of the intra-icosahedral bonds, whereas X-$(B2)_3$ vibrations result in vibration of the inter-icosahedral bonds. It should also be noted that the amplitude of the X-$(B2)_3$ vibrations are more significant at the highest frequencies, while for the $(B1)_3$ unit it is the opposite.

The A_{1g} modes of $B_{12}S$ (625.0 cm^{-1}; 761.9 cm^{-1}) and $B_{12}Se$ (645.3 cm^{-1}; 741.1 cm^{-1}) correspond to the symmetric "parasol" oscillations of X-$(B2)_3$ units, thus, resulting in distortions of the intra-icosahedral bonds. The A_{1g} modes of $B_{12}S$ (1039.2 cm^{-1}) and $B_{12}Se$ (1024.1 cm^{-1}) refer to the symmetric stretching of B–X bonds in X-$(B2)_3$ units. Finally, the A_{1g} modes of $B_{12}S$ (1093.7 cm^{-1}) and $B_{12}Se$ (1038.4 cm^{-1}) were assigned to the symmetric stretching of $(B1)_3$ units. The two latter A_{1g} modes of both boron-rich chalcogenides lead to the distortions of the inter-icosahedral bonds.

Taking into account a good agreement between theoretical and experimental data the phonon modes assignment provided above for the calculated Raman spectra of both compounds is also fear-relevant for the experimental spectra. The accuracy of the present mode assignment suffers from the noise and broad Raman bands that lead to the bands overlapping. Nevertheless, these features are rather typical for the Raman spectra of other boron-rich compounds (e.g. B_4C [61] or $B_{12}O_2$ [35]). The more precise description of the phonon modes of $B_{12}S$ and $B_{12}Se$ might be done with the help of first- and second-order Raman scattering [37].

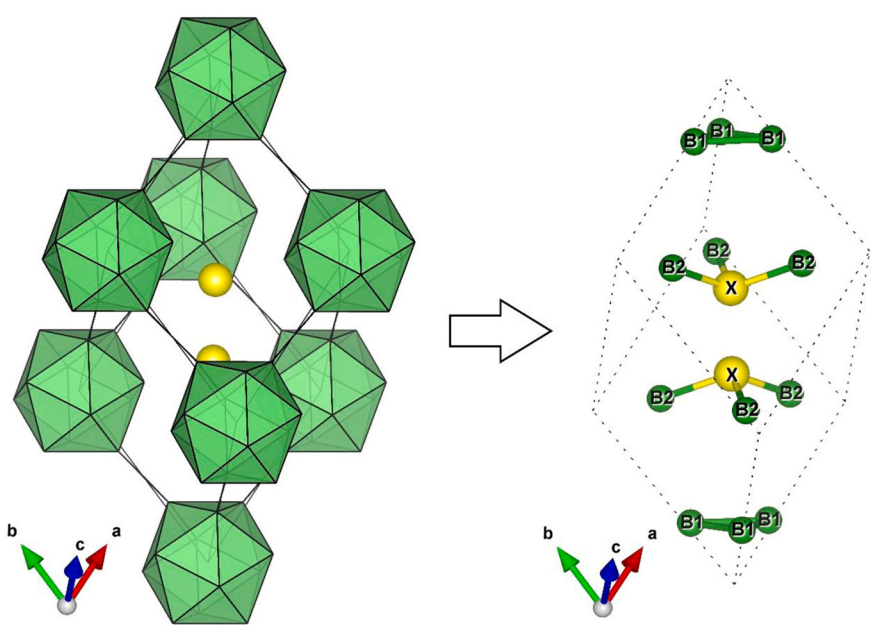

Fig. 5. $B_{12}X$ (X = S, Se) unit cell in rhombohedral setting. The polar (B1) and equatorial (B2) boron atoms of B_{12}-icosahedra are shown by green spheres, S/Se atoms are shown by yellow spheres. (For interpretation of the references to colour in this figure legend, the reader is referred to the web version of this article.)

5. Conclusions

In the present work two new stoichiometric boron-rich chalcogenides, $B_{12}S$ and $B_{12}Se$, were synthesized at high-pressure – high-temperature conditions and studied by powder X-ray diffraction and Raman spectroscopy at ambient pressure. According to the Rietveld refinement of synchrotron X-ray diffraction data, both $B_{12}S$ and $B_{12}Se$ have rhombohedral symmetry and belong to the space group *R*-3*m* (No 166). The observed Raman bands were assigned to the phonon modes and associated with the corresponding atomic movements.

CRedit authorship contributions statement

V.L.S. designed and directed the study. **V.A.M.** and **V.L.S.** performed HP-HT synthesis. **K.A.Ch.** and **V.L.S.** carried out X-ray diffraction, Raman and EDX/SEM studies. **A.K.** performed LCAO and DFT calculations. **K.A.Ch.** and **V.L.S.** analyzed the experimental data. Manuscript draft was prepared by **K.A.Ch.**; all authors discussed the results and contributed to writing and editing.

Notes

The authors declare no competing financial interest.

Declaration of Competing Interest

The authors declare that they have no known competing financial interests or personal relationships that could have appeared to influence the work reported in this paper.

Acknowledgments

The authors thank Drs. I. Dovgaliuk and T. Chauveau for assistance with Rietveld analysis; and Drs. V. Bushlya and A. Jamali for help with EDX/SEM measurements. This work was financially supported by the European Union's Horizon 2020 Research and Innovation Program under Flintstone2020 project (grant agreement No 689279).

References

[1] D.R. Armstrong, J. Bolland, P.G. Perkins, The electronic structure of α-B_{12}, $B_{12}P_2$ and $B_{12}As_2$, Theor. Chim. Acta. 64 (1984) 501–514.
[2] S. Lee, D.M. Bylander, L. Kleinman, Elastic moduli of B_{12} and its compounds, Phys. Rev. B 45 (1992) 3245–3247.
[3] F. Ding, G. Wang, S. Yu, J. Wang, W. Shen, H. Li, Formation and stability of large B_6O clusters with icosahedral structure, Eur. Phys. J. D. 16 (2001) 245–248.
[4] X. Guo, J. He, Z. Liu, Y. Tian, Bond ionicities and hardness of $B_{13}C_2$-like structured B_xX crystals, X = C, N, O, P, As, Phys. Rev. B 73 (2006) 104115.
[5] A.N. Enyashin, A.L. Ivanovskii, Structural, elastic, and electronic properties of icosahedral boron subcarbides ($B_{12}C_3$, $B_{13}C_2$), subnitride $B_{12}N_2$, and suboxide $B_{12}O_2$ from data of SCC–DFTB calculations, Phys. Solid State 53 (2011) 1569–1574.
[6] S. Veprek, R.F. Zhang, A.S. Argon, Mechanical properties and hardness of boron and boron rich solids, J. Superhard Mat. 33 (2011) 409–420.
[7] B. Wang, Z. Fan, Q. Zhou, X. Xu, M. Feng, X. Cao, Y. Wang, First principles calculations of the vibrational properties of icosahedral solid boron oxygen $B_{12}O_2$, Phys. B 406 (2011) 297–303.
[8] Z. Fan, B. Wang, X. Xu, X. Cao, Y. Wang, First-principles calculation of vibrational properties of $B_{12}As_2$ crystal, Phys. Status Solidi B 248 (2011) 1242–1247.
[9] Z. Li, F. Gao, Structure, bonding, vibration and ideal strength of primitive-centered tetragonal boron nitride, Phys. Chem. Chem. Phys. 14 (2012) 869–876.
[10] A. Ektarawong, S.I. Simak, L. Hultman, J. Birch, F. Tasnádi, F. Wang, B. Alling, Effects of configurational disorder on the elastic properties of icosahedral boron-rich alloys based on B_6O, $B_{13}C_2$, and B_4C, and their mixing thermodynamics, J. Chem. Phys. 144 (2016) 134503.
[11] A. Ektarawong, S.I. Simak, B. Alling, Thermodynamic stability and properties of boron subnitrides from first principles, Phys. Rev. B 95 (2017) 064206.
[12] B. Morosin, B. Aselage, T.L. Emin, D, On the crystal structure of boron carbides, AIP Conf. Proc. 231 (1991) 193–196.
[13] D.R. Tallant, T.L. Aselage, D. Emin, Structure of icosahedral borides by Raman spectroscopy, AIP Conf. Proc. 231 (1991) 301–311.
[14] M. Carrard, D. Emin, L. Zuppiroli, Defect clustering and self-healing of electron-irradiated boronrich solids, Phys. Rev. B 51 (1995) 11270–11274.
[15] R.J. Nelmes, J.S. Loveday, R.M. Wilson, W.G. Marshall, Observation of inverted-molecular compression in boron carbide, Phys. Rev. Lett. 74 (1995) 2268–2271.
[16] D. Emin, Unusual properties of icosahedral boron-rich solids, J. Solid State Chem. 179 (2006) 2791–2798.
[17] V.L. Solozhenko, O.O. Kurakevych, Chemical interaction in the B–BN system at high pressures and temperatures. Synthesis of novel boron subnitrides, J. Solid State Chem. 182 (2009) 1359–1364.
[18] B. Albert, H. Hillebrecht, Boron: elementary challenge for experimenters and theoreticians, Angew. Chem. Int. Ed. 48 (2009) 8640–8668.
[19] G.A. Slack, K.E. Morgan, Some crystallography, chemistry, physics, and thermodynamics of $B_{12}O_2$, $B_{12}P_2$, $B_{12}As_2$, and related alpha-boron type crystals, J. Phys. Chem. Solids 75 (2014) 1054–1074.
[20] G.A. Slack, K.E. Morgan, Crystallography, semiconductivity, thermoelectricity, and other properties of boron and its compounds, especially B_6O, Solid State Sci. 47 (2015) 43–50.
[21] V.L. Solozhenko, O.O. Kurakevich, V.Z. Turkevich, D.V. Turkevich, Synthesis of B_6O boron suboxide at pressures up to 1 GPa. J. Superhard Mater. 27 (2005) 12–16.
[22] K.A. Cherednichenko, L. Gigli, V.L. Solozhenko, Thermal expansion of boron subnitrides, Solid State Comm. 275 (2018) 21–24.
[23] K.A. Cherednichenko, V.L. Solozhenko, Thermal expansion of α-boron and some boron-rich pnictides, Solid State Commn 303–304 (2019) 113735.
[24] Orlovskaya, N.; Lugovy, M. Proc. of the NATO advanced research workshop on boron rich solids, Springer 2009.
[25] P.F. McMillan, New materials from high-pressure experiments, Nat. Mater. 1 (2002) 19–25.
[26] I. Solodkyi, S.S. Xie, T. Zhao, H. Borodianska, Y. Sakka, O. Vasylkiv, Synthesis of B_6O powder and spark plasma sintering of B_6O and B_6O-B_4C ceramics, J. Ceram. Soc. Jpn. 121 (2013) 950–955.
[27] A.R. Badzian, Superhard material comparable in hardness to diamond, Appl. Phys. Lett. 53 (1988) 2495–2497.
[28] V.A. Mukhanov, O.O. Kurakevych, V.L. Solozhenko, Hardness of materials at high temperature and high pressure, Philos. Mag. 89 (2009) 2117–2127.
[29] H.F. Rizzo, W.C. Simmons, H.O. Bielstein, The existence and formation of the solid B_6O, J. Electrochem. Soc. 109 (1962) 1079–1082.
[30] R. Sasai, R. Fukatsu, H. Kojima, T. Itoh, H, High pressure consolidation of B_6O-diamond mixtures. J. Mater. Sci. 36 (2001) 5339–5343.
[31] D. He, Y. Zhao, L. Daemen, L. Qian, J. Shen, T.D. Zerda, T.W. Boron, Suboxide: as hard as cubic boron nitride, Appl. Phys. Lett. 81 (2002) 643–645.
[32] D. Nieto-Sanz, P. Loubeyre, W. Crichton, M. Mezouar, X-ray study of the synthesis of boron oxides at high pressure: phase diagram and equation of state, Phys. Rev. B 70 (2004) 214108.
[33] D. He, S.R. Shieh, T.S. Duffy, Strength and equation of state of boron suboxide from radial X-ray diffraction in a diamond cell under nonhydrostatic compression. Phys. Rev. B 70 (2004) 184121.
[34] O.O. Kurakevych, V.L. Solozhenko, Thermoelastic equation of state of boron suboxide B_6O up to 6 GPa and 2700 K: simplified Anderson-Grüneisen model and thermodynamic consistency. J. Superhard Mat. 36 (2014) 270–278.
[35] H. Werheit, U. Kuhlmann, FTIR and FT Raman spectra of B_6O. J. Solid State Chem. 133 (1997) 260–263.
[36] Z. Wang, Y. Yusheng Zhao, P. Lazor, H. Annersten, S.K. Saxena, *In situ* pressure Raman spectroscopy and mechanical stability of superhard boron suboxide. Appl. Phys. Lett. 86 (2005) 041911.
[37] V.L. Solozhenko, O.O. Kurakevych, P. Bouvier, First and second-order Raman scattering of B_6O, J. Raman Spectrosc. 40 (2009) 1078–1081.
[38] V.L. Solozhenko, C. Lathe, On the melting temperature of B_6O. J. Superhard Mat. 29 (2007) 259–260.
[39] V. Matkovich, Interstitial compounds of boron, J. Am. Chem. Soc. 83 (1961) 1804–1806.
[40] T. Lundstrom, Structure and bulk modulus of high-strength boron compounds, J. Solid State Chem. 133 (1997) 88–92.
[41] O. Sologub, Y. Matsushita, T. Mori, An α-rhombohedral boron-related compound with sulfur: Synthesis, structure and thermoelectric properties, Scr. Mater. 68 (2013) 289–292.
[42] H. Bolmgren, T. Lundstrom, The crystal structure of a new boron selenide, $B_{12}Se_{2-x}B_x$, J. Alloy Compd. 202 (1993) 73–76.
[43] K.A. Cherednichenko, V.L. Solozhenko, Structure and equation of state of tetragonal boron subnitride $B_{50}N_2$, J. Appl. Phys. 122 (2017) 155901.
[44] K.A. Cherednichenko, Y. Le Godec, V.L. Solozhenko, Equation of state of boron subarsenide $B_{12}As_2$ to 47 GPa. High. Pres. Res 38 (2018) 224–231.
[45] K.A. Cherednichenko, V.A. Mukhanov, Z. Wang, A.R. Oganov, A. Kalinko, I. Dovgaliuk, V.L. Solozhenko, Discovery of new boron-rich chalcogenides: orthorhombic B_6X (X = S, Se), Sci. Rep. 10 (2020) 9277.
[46] V. Dyadkin, P. Pattison, V. Dmitriev, D. Chernyshov, A new multipurpose diffractometer PILATUS@SNBL, J. Synchrotron Rad. 23 (2016) 825–829.
[47] L. Lutterotti, M. Bortolotti, G. Ischia, I. Lonardelli, H.-R. Wenk, Rietveld texture analysis from diffraction images, Z. Krist. Suppl. 26 (2007) 125–130.
[48] R. Dovesi, A. Erba, R. Orlando, C.M. Zicovich-Wilson, B. Civalleri, L. Maschio, M. Rerat, S. Casassa, J. Baima, S. Salustro, B. Kirtman, Quantum-mechanical condensed matter simulations with CRYSTAL. WIREs Comput. Mol. Sci. 8 (2018) e1360.
[49] D. Vilela Oliveira, M.F. Peintinger, J. Laun, T. Bredow, BSSE-correction scheme for consistent gaussian basis sets of double- and triple-zeta valence with polarization quality for solid-state calculations, J. Comput. Chem. 40 (2019) 2364–2376.
[50] H.J. Monkhorst, J.D. Pack, Special points for Brillouin-zone integrations, Phys. Rev. B 13 (1976) 5188–5192.

[51] Z. Wu, R.E. Cohen, More accurate generalized gradient approximation for solids, Phys. Rev. B 73 (2006) 235116.
[52] A. Erba, A. Mahmoud, D. Belmonte, R. Dovesi, High pressure elastic properties of minerals from ab initio simulations: the case of pyrope, grossular and andradite silicate garnets. J. Chem. Phys. 140 (2014) 124703.
[53] Dovesi, R.; Saunders, V.R.; Roetti, C.; Orlando, R.; Zicovich-Wilson, C.M.; Pascale, F.; Civalleri, B.; Doll, K.; Harrison, N.M.; Bush, I.J.; D'Arco, P.; Llunell, M.; Causà, M. ; Noël, Y.; Maschio, L.; Erba, A.; Rerat, M.; Casassa, S. CRYSTAL17 User's Manual (University of Torino, Torino, 2017).
[54] F. Pascale, C.M. Zicovich-Wilson, F. Lopez, B. Civalleri, R. Orlando, R. Dovesi, The calculation of the vibrational frequencies of crystalline compounds and its implementation in the CRYSTAL code, J. Comput. Chem. 25 (2004) 888–897.
[55] C.M. Zicovich-Wilson, F. Pascale, C. Roetti, V.R. Saunders, R. Orlando, R. Dovesi, The calculation of the vibration frequencies of alpha-quartz: the effect of hamiltonian and basis set, J. Comput. Chem. 25 (2004) 1873–1881.
[56] H. Bolmgren, T. Lundström, S. Okada, (In AIP Conference Proceedings), Structure refinement of the boron suboxide B6O by the Rietveld method Vol. 231 American Institute of Physics, 1991, pp. 197–200 (In AIP Conference Proceedings).
[57] K.A. Cherednichenko, P.S. Sokolov, A. Kalinko, Y. Le Godec, A. Polian, J.P. Itié, V.L. Solozhenko, Optical phonon modes in rhombohedral boron monosulfide under high pressure, J. Appl. Phys. 117 (2015) 185904.
[58] K.A. Cherednichenko, Y. Le Godec, A. Kalinko, M. Mezouar, V.L. Solozhenko, Orthorhombic boron oxide under pressure: In situ study by X-ray diffraction and Raman scattering, J. Appl. Phys. 120 (2016) 175901.
[59] P. Ugliengo, D. Viterbo, G. Chiari, MOLDRAW: molecular graphics on a personal computer, Z. Krist. 207 (1993) 9–23.
[60] J.A. Shelnutt, B. Morosin, D. Emin, A. Mullendore, G. Slack, C. Wood, Raman spectroscopy of boron carbides and related boron containing materials, AIP Conf. Proc. 140 (1986) 312–324.